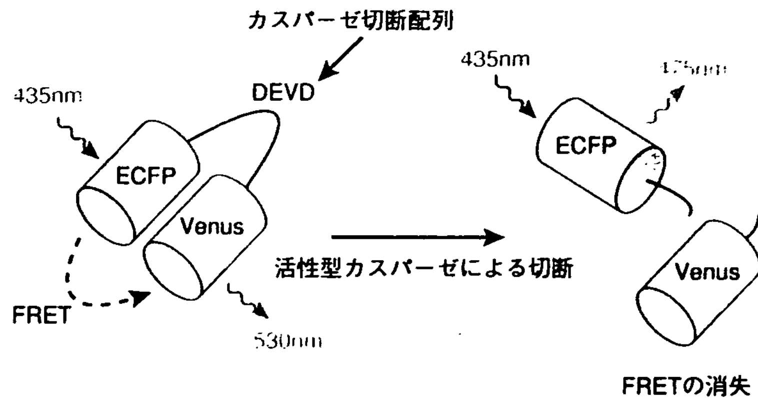

図1◆遺伝子にコードされたカスパーゼ3指示薬"SCAT3"

(Hoechst33342) 染色は細胞に容易に透過するDNA結合性の試薬であり，可視化した核構造を観察し，断片化や凝集しているものを死細胞と判定する．それに対して，TUNEL〔terminal deoxynucleotidil transferase (TdT) -mediated dUTP nick end labeling〕染色はアポトーシス細胞で認められる染色体DNAの断片化を標識することで，死細胞を検出する．断片化したもののみ染色されるため，死細胞のカウントやパターンを検出するのに適していると考えられる．

2. ホスファチジルセリンの検出

また，細胞死の初期段階においては，細胞膜の内側に局在する陰性荷電リン脂質のホスファチジルセリン (PS：phosphatidyl serine) が細胞表面に露出する．Ca^{2+}依存性のリン脂質結合タンパク質であるAnnexin VはPSに選択的に結合するため，蛍光ラベルしたAnnexin Vを用いて細胞死の検出が可能である．Annexin染色は操作が比較的簡便であり，フローサイトメトリーを用いた解析でも広く用いられている．以上の試薬は簡便ですでに広く使われており，細胞死研究になくてはならない手法として確立されている．

それでは個体レベルの細胞死のすべてを上記の方法で検出できるかといえば，それは困難と言わざるを得ない．個体内では，死細胞はマクロファージなどの貪食細胞ですみやかに除去されることが知られているからである．したがって個体における細胞死のパターンを知るためには，生きたままリアルタイムに検出する方法が求められる．しかしながら，従来の方法では，生きたまま長時間死細胞を検出することは非常に困難であった．

FRETを利用した観察

1. cDNAにコードされたカスパーゼ指示薬

生体内で生きたまま分子の機能を解析するための強力な手段として蛍光タンパク質を用いたFRET（フェルスター共鳴エネルギー移動）を利用する方法が注目されている．FRETを利用することで時空間的な分子の解析ができ，これまでさまざまな分子に対する指示薬が開発されてきた．FRETの原理に関しては第Ⅱ部4章-❺を参照していただきたい．活性型カスパーゼ3に対する指示薬（SCAT3）はFRETのドナーにECFPを，アクセプターにVenusを用い，両分子間にカスパーゼ3の至適切断配列(DEVD) を含むリンカー配列が挿入されている (図1)．カスパーゼ3により切断される前（左側）はドナー (ECFP) からアクセプター (Venus) へFRETが起こる（図1左）が，切断後（図1右）にはFRETが消失する．本指示薬はcDNAにコードされているため，適当な方法を用いて個体内の特異的な細胞や組織に発現させ，リアルタイムにカスパーゼ活性や細胞死を検出することが可能になった[1)～4)]．

2. YFPを用いる際の注意点

ところで，生きた細胞内でのカスパーゼ活性化の

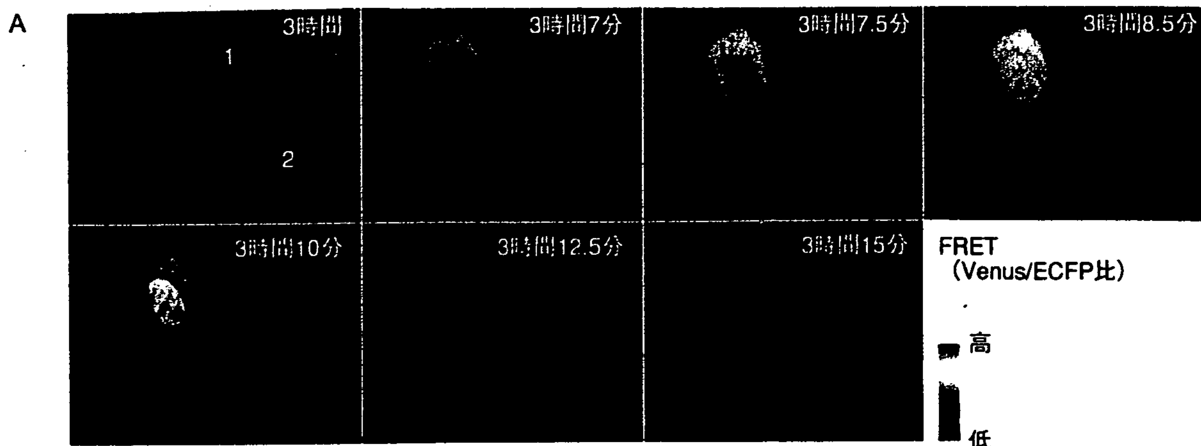

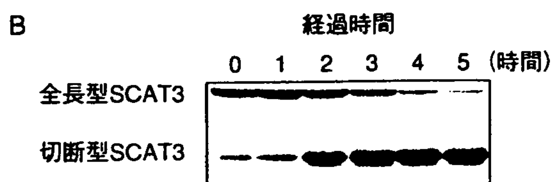

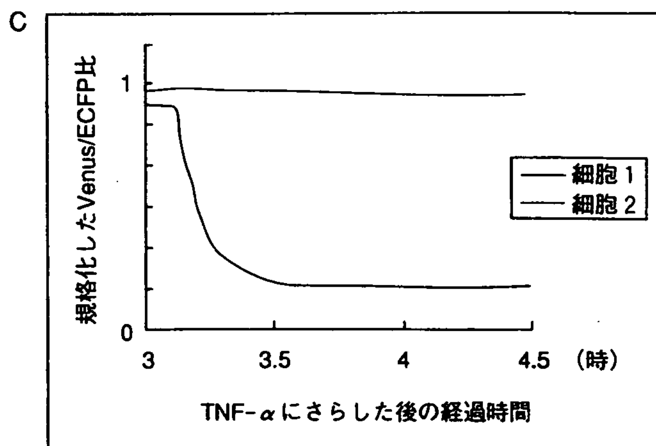

図2◆SCAT3を用いた生細胞でのライブイメージング

定量的検出を行うには，従来用いられてきたECFP-EYFPペアでは不充分であると考えられる．というのも，アクセプターEYFPのモル吸光度はプロトンやクロライドイオンに対し，感受性が非常に高いためである．アクセプターのモル吸光度はFRETの重要な因子であり，こうした因子の変動に由来する，つまりカスパーゼ以外の偽シグナルを受ける可能性が示唆される．アポトーシス実行過程では，細胞質やミトコンドリアにおけるpHの変動が報告されている．また神経系の細胞では活動依存的にプロトン濃度の変動が報告されている．さらにはEYFP発現マウスを用いて，こうした因子の変動が観察されることも報告されている．以上のことから，特に生きた細胞内でFRET観察をする際，YFPをアクセプターに用いるのは慎重を期すべきであろう．生理的な濃度の変動範囲内ではVenusの蛍光強度は両イオンにほとんど影響を受けないため，FRETアクセプターとしてはEYFPよりもVenusの方が優れている．

⃞ SCAT3を用いた生きた細胞におけるカスパーゼ活性化のライブイメージングの実験例

SCAT3は遺伝子にコードされた機能指示薬であることから，化学合成プローブでは困難なオルガネラなどの細胞の局所に発現させることが容易であり，細胞の局所的なカスパーゼ活性を詳細に解析できる．また，組織特異的プロモーターを用いてプローブを見たい細胞のみに発現させることが可能であり，個体レベルでのイメージングに適していると言える．図2-AはヒトHeLa細胞にSCAT3を発現させ，細胞死誘導因子TNF-αを添加した際の，カスパーゼ活性化のライブイメージングを示している．一般的にはFRET（ここではVenus/ECFP蛍光強度比で換

- ライブイメージングでなくとも，固定標本でもSCAT3を用いたカスパーゼ活性化検出は可能である．通常カバーガラス上に培養した細胞を4%ホルマリン/PBSで固定し，市販のマウント剤を用いてスライドガラス上に固定標本を作製することで観察できる．ところがこうしたマウント剤で長時間（おおよそ1日以上）保存すると，標本作製直後と比較してVenus/ECFP蛍光強度比が低下してしまうことがある．つまり本来カスパーゼ活性化が起こっていない細胞で，あたかもカスパーゼ活性が高いように観察されうる．

- すべての市販のマウント剤を試したわけではないが，少なくともマウント剤をPBSに変えると，この問題はほとんど起こらなくなる．おそらくマウント剤の成分のうち，CFPと比較してYFPの蛍光特性にいくらかのダメージを与える物質があると予想される．いずれにせよプローブを観察する環境は，アクセプターもドナーもその蛍光特性に変化がないことが定量的観察の前提である．これは前述のYFPのイオン感受性の問題にも通ずるところがある．同じ蛍光タンパク質といえども発色団構造の違いからその特性は全く異なるものになるため，2種類の蛍光タンパク質を使うFRETにおいては，その特性を充分に理解して使用することが特に必要である．

算）の変動を示す際，図のような擬似カラー表示をし，空間的な情報の解析を行う．

このように，SCAT3を用いることで細胞や核が形態変化を見せる前に，カスパーゼ活性化を検出することができる．すなわち「プレ死細胞」を検出できるといえる．カスパーゼの活性化は細胞質で起こり，核へと伝播することが明らかになった．また，カスパーゼの活性化は多くの細胞をすり潰すことにより行う生化学的な解析（例えば，抗活性型カスパーゼ抗体によるウエスタンブロット）からは，徐々に活性化が進行していくと考えられていた（図2-B）が，1細胞レベルのイメージングによる解析からは，活性化がはじまる時刻が個々の細胞ごとに異なり，かつ“all or none”のパターンで活性化することが明らかになった（図2-C）．このように，ライブイメージングでは従来の手法でわからなかった個々の細胞の個性・ダイナミクスを解析することができる．

おわりに

本項ではアポトーシスを検出する主な手法を解説した．いずれの手法にも利点と欠点があり，それぞれの原理と利点をよく理解して使用することが大切である．顕微鏡下におけるFRETの検出・ライブイメージングの実際のプロトコールは他書[5]を参照していただきたい．

参考文献

1）Takemoto, K. et al. : J. Cell Biol., 160 : 235-243, 2004
2）Kanuka, H. et al. : EMBO J., 24 : 3793-3806, 2005
3）Kuranaga, E. et al. : Cell, 126 : 583-596, 2006
4）Tekemoto, K. et al. : Proc. Natl. Acad. Sci. U. S. A., 104 : 13367-13372, 2007
5）永井健治，宮脇敦史：『分子生物学実験シリーズ　図・写真で観るタンパク構造機能解析実験実践ガイド』（月原富武，新延道夫/編），pp. 173-182, メディカルドゥ, 2005

スパイはひとりで充分　蛍光タンパク質を用いた蛍光1分子イメージング

生きた細胞内におけるタンパク質の所在やその振る舞い，機能に伴う分子同士の会合を観察するために，蛍光タンパク質は広く用いられている．タンパク質の挙動のみならず，細胞内におけるイオン濃度などをモニターする目的においても，蛍光タンパク質の活躍はめざましい．このような細胞内イメージングのために，われわれは本来生体内には存在しないタンパク質を発現させている．正常な細胞機能を観察するためには，その発現量は少ないほどよい．スパイはふつうごく少人数で敵国に潜入し，得られた情報を本国に報告するものだ．そこで，生体内に送り込んだ少数のスパイ蛍光タンパク質を観察する，蛍光1分子イメージング技術の必要性が生まれてくる．明るさや光安定性の点から，これまで蛍光1分子イメージングにはCy3やローダミンなどが好まれて用いられてきた．しかしながら近年の光学顕微鏡およびその周辺機器の進歩，特に撮像素子の感度やシグナル/ノイズ比の向上により，蛍光タンパク質を用いた蛍光1分子イメージングは標準的な実験技術になろうとしている．

1分子イメージングで観察可能な分子の濃度の上限はせいぜい数nMである．いわゆる"漏れ"の少ないInducible promoter〔例えばNEB（New England Biolaps社）のRheoSwitch®システムなど〕を用いることにより，発現量を充分に抑えることが必要であろう．比較的弱い蛍光シグナルを検出するために，カバーガラスの洗浄，蛍光の少ない油浸オイルや培養液の選択，細胞がもつ自家蛍光の波長帯域からはずれた蛍光タンパク質の選択なども考慮する必要がある．われわれの経験では，蛍光1分子観察に充分な光安定性をもつ蛍光タンパク質（モノマー）として，EGFPやmCherryがあげられるが，今後これらを凌ぐ光安定性をもち，明るい蛍光タンパク質が出現することは間違いないだろう（谷　知己，永井健治）

4章　細胞・酵素活性測定のためのプローブ
❺ FRETプローブ
—蛍光分子の組合わせ選択から分子間距離の計算法まで

永井健治，小寺一平
Takeharu Nagai, Ippei Kotera

はじめに

「タンパク質Aとタンパク質Bが相互作用する」このような結論を言いたいがために，多くの実験をこなさなければならず，頭を抱え込んでいる読者は多いであろう．さらに「生きた細胞の中で」という条件がここに含まれると非常にチャレンジングな研究課題になることは誰の目にも明らかである．生細胞を観察する手段としては光学顕微鏡が最も一般的であるが，通常の顕微鏡ではタンパク質の相互作用を直接観察することができない．可視光を利用する光学顕微鏡の分解能は光の回折限界により制限され，通常の条件で達成可能な空間分解能は数百nm程度に過ぎないからである．この空間分解能で直径数nmのタンパク質の相互作用を観察しようとするのは，例えれば，「肉眼でHeLa細胞の核小体の融合を観察する」ようなものである（肉眼の空間分解能は0.1～0.3mm，核小体の大きさは1～3μm程度）．

Förster共鳴エネルギー移動（FRET）と呼ばれる物理現象を用いれば，このような空間分解能以下の分子動態を観察することが可能になる．FRETとは，ドナー分子が励起状態にあり，かつアクセプター分子が基底状態のときに起こる，光放射を伴わないドナーからアクセプターへのエネルギー移動のことをいう[1]．この現象を蛍光スペクトルや蛍光寿命の変化として捉えることで，さまざまな生体高分子の動態やタンパク質の機能変化などが可視化されてきた[2]．特に，蛍光タンパク質と遺伝子工学を駆使したFRETイメージングは，生細胞内の遺伝子産物を動的に観察する際の強力なツールへと発展し，人口に膾炙したと言っても過言ではない．その反面，こうしたツールを使いこなすためには従来の生化学や分子生物学以外のノウハウが必要であり，誰でも使いこなせる技術にまで成熟していないことも確かである．誰もが理解できるやさしいノウハウ本の出現が期待されているなか，本項ではFRET実験を行う際の基本中の基本である，ドナー/アクセプターペアの選択法からFRETの測定結果に基づく分子間距離を求める手順までを平易に解説することを心掛けた．読者の一助になれば幸いである．

FRETペアの選択基準

FRETは，ドナー/アクセプター間の距離とスペクトルの重なり積分，配向，ドナーの蛍光量子収率に依存する．FRET効率が50%になるときのドナーとアクセプターとの間の距離をFörster距離（R_0）と呼び，以下の式で求められる．

$$R_0 = 9.78\times10^2(\kappa^2 n^{-4} Q_D J)^{1/6} \quad \cdots式1-1$$

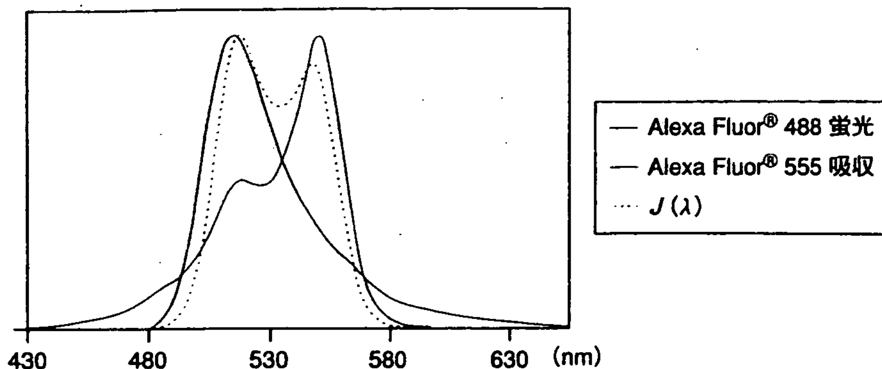

図1◆重なり積分（J）の模式図

κ^2は配向因子，nは媒質の屈折率，Q_Dはドナーの蛍光量子収率，Jはドナーの蛍光とアクセプターの吸収の重なり積分を表す．ここで注目すべきは，Förster距離のスケールである．細胞観察で一般に用いる条件では，Förster距離は5 nm程度となり，生体高分子のスケールと一致する．生体内の分子動態の可視化にFRETが適している所以である．

また実際のFRET効率（E）は，

$$E_0 = \frac{1}{1+(r/R_0)^6} \qquad \cdots式1-2$$

で求められる．ここで，rはドナー/アクセプター間の実際の距離であり，FRET効率はドナーとアクセプターとの間の距離の6乗に反比例することがわかる．これらのことから言えることは，タンパク質などに導入された蛍光色素がR_0の距離にあるときに50%のFRET効率が得られ，また，距離の変化に対して非常に感受性が高い（距離の6乗に反比例する）ということである．あるいは，タンパク質Aとタンパク質Bが非常に近接した状態（相互作用している状態）でエネルギー移動が起こり，タンパク質Aとタンパク質Bの距離がわずかでも変化すると，FRET効率が鋭敏に変化するといってもよい．

細胞の中でFRETを検出する際に，FRET効率が高すぎて困ることはない．むしろFRET効率が小さくて検出が困難なことがほとんどである．このため，できるだけFRETの起こりやすいドナーとアクセプターのペアを選択することが重要となる．FRETが起こりやすいペアは，Förster距離が大きいペアである．式1－1をもう一度見てみると，分子の配向（κ^2）に関しては，発色団の配向を実験的に変化させてFRET効率を向上させることが可能[3]であるが，計算で分子の配向を決定することは困難である．また，細胞内の屈折率（n）は任意に変えられないことから，ドナーとアクセプターのペアを選択する際には，Q_DとJの値を考慮することが重要になる．

Jは，ドナーの蛍光スペクトルとアクセプターの吸収スペクトルとの重なり積分（図1）のことで，次の式で求められる．

$$J = \int_0^\infty F_D(\lambda)\varepsilon_A(\lambda)\lambda^4\delta\lambda \qquad \cdots式1-3$$

F_Dはドナーの全蛍光スペクトルの強度を1に規格化したときの各波長における蛍光強度の値，ε_Aはアクセプターのモル吸光係数（$M^{-1}cm^{-1}$），λは光の波長（cm）である．Jの単位は$M^{-1}cm^3$になる．FRETプローブを作成する前に候補ペアの重なり積分（J）を求めることで，FRETペアの膨大な組合わせを理論的に絞り込むことができる．

計算の方法

重なり積分（J）とFörster距離を計算をするた

めには，まずそれぞれのスペクトルデータを入手する必要がある．実際のサンプルが手元にない場合は，Webなどで公開されているスペクトルデータを参照する．

PubSpectra（http://home.earthlink.net/~pubspectra/）では，多種多様な蛍光分子のスペクトルが公開されているが，ここで必要なのはドナーの蛍光スペクトルとアクセプターの吸収スペクトルである．

計算には，マイクロソフトのExcelを用いる．Excel以外でも，簡単な関数が扱える表計算ソフトであれば同様のことはできる．また，本項で解説している計算シートは，当研究室のホームページ（http://nano.es.hokudai.ac.jp/）で公開している．一例として，ここではAlexa Fluor® 488とAlexa Fluor® 555（販売元：インビトロジェン社）における重なり積分（J）とFörster距離（R_0）を実際に求めてみる（図2）．

①表計算シートの任意の列に300nmから700nmまでの波長を1nmごとに列記する．例えばA5のセルに300と入力し，連続データの作成機能などを使ってA406のセルまで連続データを入力する．

②ドナー（Alexa Fluor® 488）の蛍光スペクトルをBの列に入力する．値のないセルは空白のままで構わない．例えば480nmから674nmの蛍光スペクトルであれば，B185からB379にそれぞれの値を入力する．

③Cの列で，全蛍光量で規格化した蛍光強度を計算する．C5のセルに「=B5/SUM（B：B）」と入力することで計算できる．C405まで下方向にコピーすると各波長に対応した計算式が自動的に入力される．

④Dの列にアクセプター（Alexa Fluor® 555）の吸収スペクトルを入力する．

⑤吸収スペクトルが規格化されていない場合は，E5のセルに「=D5/MAX（D：D）」の計算式で規格化する．計算式を下方向にコピーし，各波長分

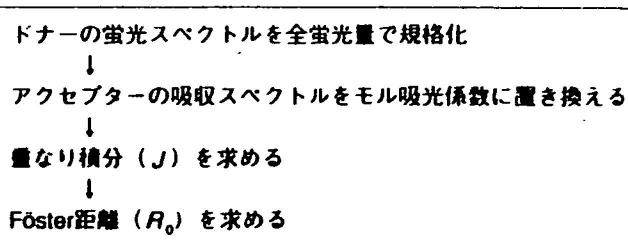

図2◆計算のながれ

を入力する．

⑥Fの列にアクセプターの最大モル吸光係数を入力する．Alexa Fluor® 555の場合，158000と入力し，同じ値をF5からF405まで入力する．

⑦Gの列で各波長でのモル吸光係数を計算する．G5に「=E5*F5」と入力し，G405まで下方向にコピーすることで，それぞれの波長に対応した数式を入力する．

⑧Hの列に波長をnmからcmに変換する式を入力する．H5に「=A5*1e-9/1e-2」と入力してH405まで下方向にコピーする．

⑨Iの列で，式1－3に従い各波長での$J(\lambda)$を求める．I5のセルに「=C5*G5*POWER（H5,4）」と入力し，I405まで下方向にコピーする．

⑩$J(\lambda)$を合計し，Jを求める．J5に「=SUM（I：I）」と入力する．

⑪K5のセルに「=2/3」と入力して配向因子（κ^2）とする．

⑫L5のセルに「=power（1.33, -4）」と入力して屈折率の－4乗（n^{-4}）とする．

⑬M5のセルにドナーの量子収率（Q_D）を入力する．Alexa Fluor® 488の場合は，0.92とする．

⑭式1－1に従ってFörster距離を求める．N5に「=9.78*100*POWER（J5*K5*L5*M5,1/6)」と入力して計算する．

どうであろう？ Alexa Fluor® 488とAlexa Fluor® 555の重なり積分（J）が$5.96 \times 10^{-13} M^{-1} cm^3$，Förster距離（$R_0$）が6.8nmとなっているはずである．われわれの経験則では，Jが$1 \times 10^{-13} M^{-1} cm^3$を超えるとFRET観察が容易になるとの感覚がある

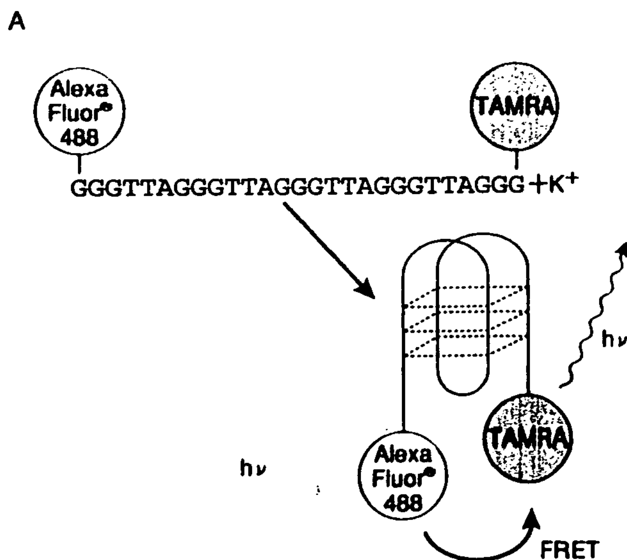

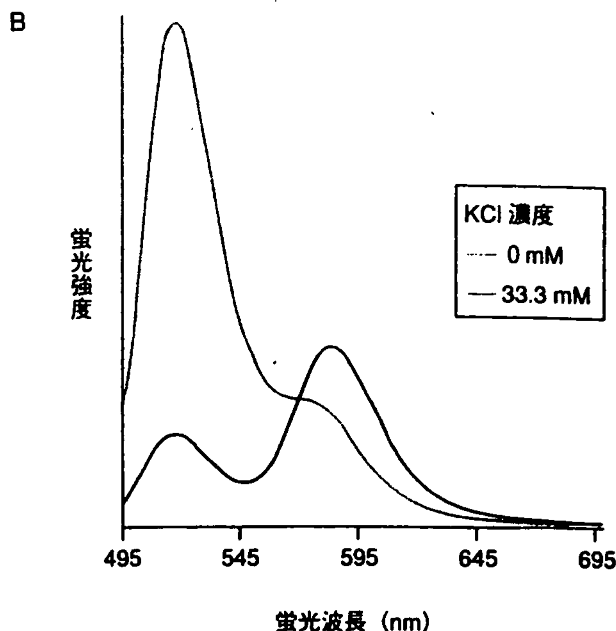

図3◆陽イオン感受性オリゴDNA
テロメア繰り返し配列のK^+添加による立体構造変化とAlexa Fluor® 488からTAMRAへのFRETの誘起（A）およびそれに伴う蛍光スペクトルの変化（B）

ので，この値はFRETペアとしてかなり優秀な数字であるといってもよいであろう．

実験例―テロメア配列の構造変化観察

テロメアDNAはTTAGGGの繰り返し配列をもち，陽イオン存在下でG-quadruplexと呼ばれる四本鎖構造を形成する[4]．このテロメアDNAの両端に蛍光色素を結合し（図3-A），陽イオン添加前後で蛍光スペクトルの変化を観察することで，蛍光色素間の距離の変化をFRET効率の変化として捉えた．

33mMのKClを加えてテロメアDNAが高次構造を形成すると蛍光色素間の距離が小さくなり，ドナーの蛍光強度が小さくなる（図3-B）．

このときのFRET効率は，以下の式によって計算できる．

$$E = 1 - \frac{F_{DA}}{F_A} \qquad \cdots 式1-4$$

F_{DA}はアクセプター存在下でのドナーの蛍光強度，F_Dはドナーのみの蛍光強度である．式1－4にそれぞれの値を代入すると，高次構造を形成したときの色素間のFRET効率は64.5%であることが計算できる．また上記で紹介した計算方法によりこのペアのR_0が求められるので，式1－2から色素間の距離は5.5nmと計算できる．

おわりに

このように，（やってみれば意外と）簡単な測定と計算で，光学顕微鏡の分解能よりもはるかに小さな分子の動態を光で捉えることができるのである．生物学のメインストリームの研究者がこのようなテクニックを使うようになれば，回折限界の壁に隠されている未知の現象がますます明らかになっていくに違いないであろう．

●比較的簡単にFRETペアの相性を計算することができるので，ぜひ一度他の蛍光分子に関しても試してみてもらいたい．重なり積分やFörster距離はFRETペアを選択するうえで非常によい指標となるが，もちろんこれらの指標以外にも，蛍光ラベルを複数選択する際の通常の指標も同時に考慮しなくてはならない．すなわち，多蛍光色素間でのクロストークや，観察機材との相性，褪色に対する安定性，イオン感受性などである．これらについては，参考文献5に詳しい．

●理論と実験結果が一致しないのは世の常である．実験で得たFRET効率が理論値を上回ることはあまりないが，下回ることは頻繁にある．蛍光色素の多くは，タンパク質などに共有結合させると蛍光量子収率が下がることが報告されている．また，立体障害により，蛍光強度が大きく下がることもあり，目的のアクセプター以外へのエネルギー移動（クエンチング）が起こることもある．いずれにしても，実験でより多くの条件を試すことが重要であることは論を待たない．

●前述の式1－3のλ^4について補足すると，これは長波長の蛍光色素がFRETに有利であることを示唆している．先ほどの計算シートで，λの値を200nm程長波長側にずらしてみるとよい．Förster距離が大幅に増加するはずである．Jはλの4乗に比例するため，λが20％ほど増加するだけでJは2倍程度に上昇する．一般的に，長波長領域の色素はモル吸光係数が高いので，さらに有利な条件が得られる．他の状況が許せば，より長波長側のペアを選択することは理にかなっていると言えよう．

参考文献

1）宮脇敦史：実験医学, 18：1111-1119, 2000
2）Miyawaki, A.：Dev. Cell, 4：295-305, 2003
3）Nagai, T. et al.：Proc. Natl. Acad. Sci. U. S. A., 101：10554-10559, 2004
4）Ueyama, M. et al.：J. Am. Chem. Soc., 124：14286-14287, 2002
5）永井健治，宮脇敦史：『図・写真で観るタンパク構造機能解析実験実践ガイド』（月原冨武，新延道夫），メディカルドゥ社，pp.173-182, 2005

Cell

SCRAPPER-Dependent Ubiquitination of Active Zone Protein RIM1 Regulates Synaptic Vesicle Release

Ikuko Yao,[1] Hiroshi Takagi,[1] Hiroshi Ageta,[1] Tomoaki Kahyo,[1] Showbu Sato,[1] Ken Hatanaka,[1] Yoshiyuki Fukuda,[2] Tomoki Chiba,[3,7] Nobuhiro Morone,[4] Shigeki Yuasa,[4] Kaoru Inokuchi,[1] Toshihisa Ohtsuka,[5] Grant R. MacGregor,[6] Keiji Tanaka,[3] and Mitsutoshi Setou[1,2,*]
[1]Mitsubishi Kagaku Institute of Life Sciences (MITILS), 11 Minamiooya, Machida, Tokyo 194-8511, Japan
[2]National Institute for Physiological Sciences, 5-1 Higashiyama, Myodaiji-cho, Okazaki, Aichi 444-8787, Japan
[3]Laboratory of Frontier Science, The Tokyo Metropolitan Institute of Medical Science, 3-18-22 Honkomagome, Bunkyo-ku, Tokyo 113-8613, Japan
[4]Department of Ultrastructural Research, National Institute of Neuroscience, National Center of Neurology and Psychiatry, 4-1-1 Ogawahiigashi-cho, Kodaira, Tokyo 187-8502, Japan
[5]Department of Clinical and Molecular Pathology, Faculty of Medicine/Graduate School of Medicine, University of Toyama, Sugitani 2630, Toyama 930-0194, Japan
[6]Department of Developmental and Cell Biology, and Center for Molecular and Mitochondrial Medicine and Genetics, University of California, Irvine, CA 92697-3940, USA
[7]Present address: University of Tsukuba, Graduate School of Life and Environmental Sciences, 1-1-1 Tennodai, Tsukuba, Ibaraki 305-8577, Japan.
*Correspondence: setou@nips.ac.jp
DOI 10.1016/j.cell.2007.06.052

SUMMARY

Little is known about how synaptic activity is modulated in the central nervous system. We have identified SCRAPPER, a synapse-localized E3 ubiquitin ligase, which regulates neural transmission. SCRAPPER directly binds and ubiquitinates RIM1, a modulator of presynaptic plasticity. In neurons from *Scrapper*-knockout (SCR-KO) mice, RIM1 had a longer half-life with significant reduction in ubiquitination, indicating that SCRAPPER is the predominant ubiquitin ligase that mediates RIM1 degradation. As anticipated in a RIM1 degradation defect mutant, SCR-KO mice displayed altered electrophysiological synaptic activity, i.e., increased frequency of miniature excitatory postsynaptic currents. This phenotype of SCR-KO mice was phenocopied by RIM1 overexpression and could be rescued by re-expression of SCRAPPER or knockdown of RIM1. The acute effects of proteasome inhibitors, such as upregulation of RIM1 and the release probability, were blocked by the impairment of SCRAPPER. Thus, SCRAPPER has an essential function in regulating proteasome-mediated degradation of RIM1 required for synaptic tuning.

INTRODUCTION

During neuronal communication, synaptic vesicles dock and fuse with the plasma membrane of the presynaptic (transmitting) neuron at sites called "active zones." Subsequently, neurotransmitters released into the extracellular synaptic space can bind to cell surface receptors located at sites on the postsynaptic (receiving) cell called "postsynaptic densities." Both of these specialized intracellular sites contain complexes of scaffolding proteins, neurotransmitter-releasing machinery, receptors, ion channels, and signaling molecules that facilitate synaptic transmission and subsequent signal transduction (Hata and Takai, 1999; Sudhof, 2004; Yao et al., 1999). Modulation of the activity of such protein complexes is important for control of synaptic plasticity. It is not yet fully understood how the activity of these synaptic proteins is regulated, but this sophisticated process includes control at the level of transcription (Bito et al., 1996), translation (Kosik, 2006), and translocation (Ikegami et al., 2007; Matsumoto et al., 2007; Setou et al., 2000, 2002).

Recently, protein degradation has attracted attention as a mechanism to control the level of synaptic proteins. Protein degradation mediated by the ubiquitin-proteasome system (UPS) (Coux et al., 1996; Hershko and Ciechanover, 1998; Varshavsky, 2005) functions in a variety of cellular processes (Pickart, 2001; Varshavsky, 2005). Target proteins are tagged with polyubiquitin via UPS enzymes and then degraded in the proteasome. By controlling the stability, activity, and localization of

synaptic proteins, UPS provides an additional mechanism for control of synaptic function. For example, UPS machinery can modulate the level of synaptic proteins such as Vesl-1S/Homer-1a (Ageta et al., 2001), serum-inducible kinase (SNK) (Pak and Sheng, 2003), anaplastic lymphoma kinase (ALK) (Liao et al., 2004), synaptophysin (Wheeler et al., 2002), and syntaxin1 (Chin et al., 2002). Furthermore, it has been suggested that activity-dependent regulation of synaptic function in vivo can be regulated by UPS at both pre- and postsynapses (Ehlers, 2003; Yi and Ehlers, 2005). Indeed, optical analysis of synaptic vesicles indicates that inhibition of proteasome activity triggers a presynaptic modulation in cultured hippocampal neurons (Willeumier et al., 2006). However, the molecular mechanisms whereby UPS regulates synaptic transmission in vivo are unknown.

We have identified SCRAPPER, an ubiquitin ligase found in mammalian CNS synapses and have analyzed its function in synaptic transmission. SCRAPPER directly binds to and ubiquitinates the active zone protein Rab3-interacting molecule 1 (RIM1) in vitro and in vivo. Analysis of mice mutant for SCRAPPER demonstrates that SCRAPPER-dependent UPS contributes to the regulation of synaptic vesicle release probability via RIM1.

RESULTS

SCRAPPER Is a Neural E3 Ubiquitin Ligase Localized on Presynaptic Membrane

Protein ubiquitination involves three classes of enzymes: ubiquitin-activating enzyme (E1), ubiquitin-conjugating enzymes (E2), and ubiquitin-protein ligases (E3). Specificity in ubiquitination is often conferred by E3 enzymes due to their high-substrate specificity. We hypothesized that an E3 capable of regulating synaptic function would be membrane bound and would be expressed in neurons. To test this hypothesis we screened the human genome for genes whose coding sequence contained an F box domain (characteristic of E3 ligases), a membrane-targeting sequence, and whose promoter region contained both a neuron-restrictive silencing element and a cAMP-response element (CRE) within 3 kb upstream of exon 1. Only one gene was found with all of these properties. We cloned a full-length cDNA for the mouse ortholog and named the encoded protein "SCRAPPER." SCRAPPER is a 438 amino acid protein that contains an F box, leucine-rich repeats (LRR), and a CAAX domain. The CAAX domain is a carboxyl-terminal membrane-sorting signal induced by prenylation (Zhang and Casey, 1996).

We verified that SCRAPPER has these properties in vivo. Cyclic-AMP responsive expression of *Scrapper* mRNA was observed in primary culture of hippocampal neurons 1 hr following induction by forskolin (a cAMP signaling activator) (Figure S1). Western analysis of levels of SCRAPPER in the mouse brain revealed a gradual increase with age, from midgestation to adult (Figure S2A). In adult mice, highest levels of SCRAPPER were observed in the brain (Figure 1A), where it appeared evenly distributed (Figure S2B). Analysis using in situ hybridization (Figure 1B) and immunohistochemistry (Figure 1C) revealed that *Scrapper* mRNA and protein were enriched in the CA1, CA3, and dentate gyrus regions of the hippocampus, as well as in the cerebellum and olfactory bulb. Subcellularly, SCRAPPER was enriched in synaptic membrane fractions from the mouse brain (Figure 1D). Immunofluorescence analysis revealed a punctate distribution of SCRAPPER (Figure 1F) that predominantly colocalized with synaptophysin, a known synaptic vesicle protein and presynapse marker. GFP-tagged full-length SCRAPPER (GFP-SCR) was distributed in a punctate manner similar to endogenous SCRAPPER (Figures 1E and 1F). In contrast, GFP-SCR-C435A, which carries a mutation in the CAAX motif, had more diffuse distribution than those observed for wild-type GFP-SCR and -SCR-CAAX. This indicates that the carboxyl-terminal prenylation signal is important for the distinct localization of SCRAPPER. GFP-SCR-LRR, which we expected to have a dominant-negative effect due to presence of the LRR target protein-binding domain, but without the F box or CAAX domains, also displayed a diffuse subcellular distribution (Figure 1F).

SCRAPPER Acts as an E3 Ubiquitin Ligase for RIM1 In Vitro

F box-containing proteins are a component of the multisubunit RING-finger type SCF complex (Cardozo and Pagano, 2004), which acts as an E3 enzyme. Similarly, SCRAPPER formed an SCF complex with Skp1 and Cullin1 in mouse brain lysates (Figure 2A). Consistent with a function as a ubiquitin ligase, ubiquitinated proteins coimmunoprecipitated (co-IPed) with FLAG-tagged SCRAPPER (FLAG-SCR) from lysates of MG132-treated (a proteasome inhibitor) cells (Figure 2B). These ubiquitinated proteins may include target proteins and/or autoubiquitinated SCRAPPER. Due to the colocalization of SCRAPPER with synaptophysin (Figure 1F), we screened the SCRAPPER IPs for known presynaptic proteins (Figure 2C). RIM1, a Ca^{2+}-dependent synaptic vesicle-priming factor in the active zone that is required for synaptic plasticity (Wang et al., 1997), co-IPd with SCRAPPER (Figure 2C). SCRAPPER partially colocalized with RIM1 in cultured neurons (Figure 2D). Purified recombinant SCRAPPER and C2B domain of RIM1 directly interacted in an in vitro pull-down assay (Figures 2E and S3). Furthermore, in IPs of native SCRAPPER from the mouse brain, RIM1 was shifted to a higher molecular weight after the addition of a ubiquitination priming mixture (E1, E2, ubiquitin, and a NEDD8 system [Kawakami et al., 2001]) (Figure 2F). Thus, the SCRAPPER complex was sufficient to mediate ubiquitination of RIM1 in vitro.

SCR-KO Mice Have Deficiency in RIM1 Ubiquitination, Prolonged Half-Life of RIM1, and Increased Steady-State Levels of RIM1

To investigate the physiological function of SCRAPPER, we generated *Scrapper*-knockout (SCR-KO)- and *Scrapper*-transgenic (SCR-TG) mice in which the expression

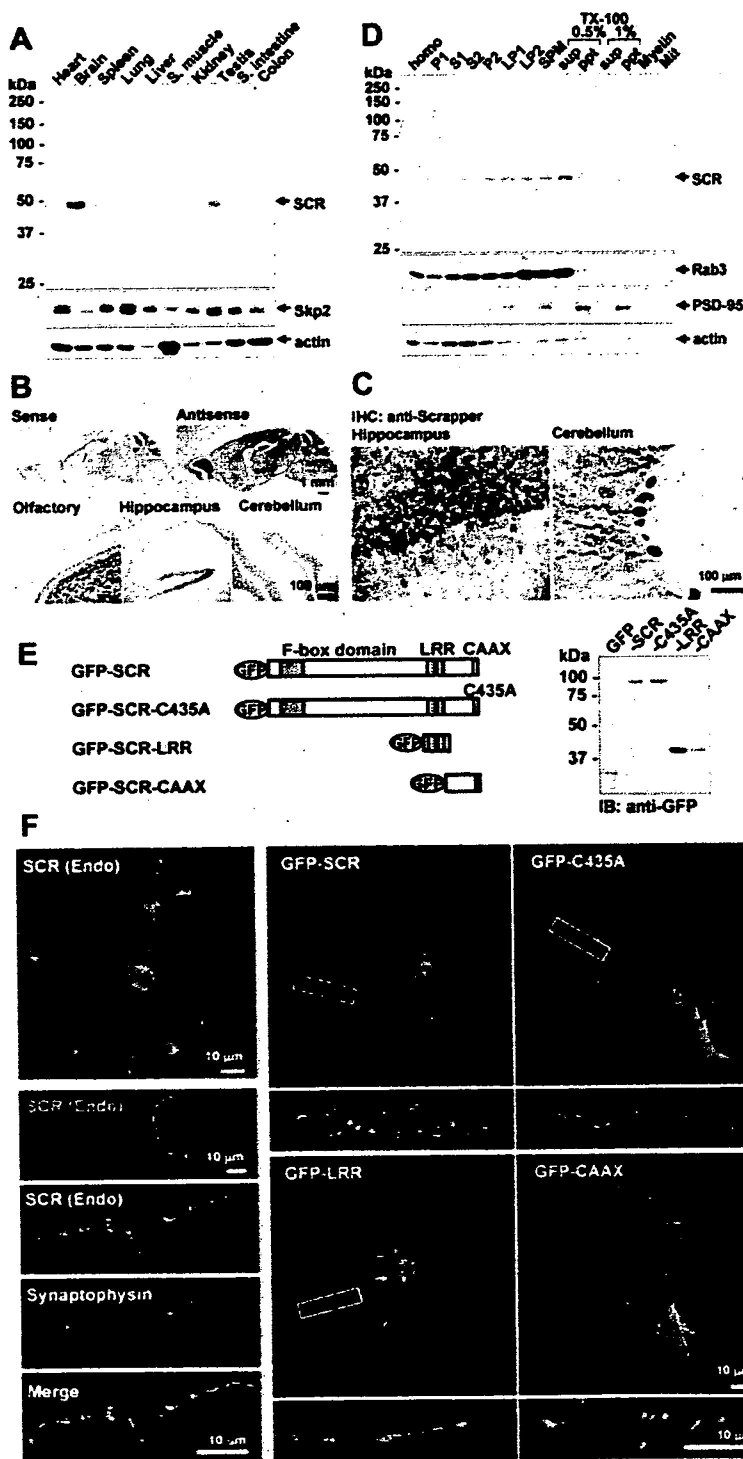

Figure 1. SCRAPPER Is a Neuronal E3 Ligase
(A) Tissue distribution of SCRAPPER protein.
(B) In situ hybridization analysis of *Scrapper* mRNA.
(C) Immunohistochemical analyses of SCRAPPER distribution in mouse cerebellum and hippocampus.
(D) Subcellular distribution of SCRAPPER in the brain. SCRAPPER was present in membrane fractions, especially synaptosomal membrane (SPM) fraction and the 0.5% (w/v) Triton X-100-soluble fraction of the SPM. Homo, the homogenate fraction. In (A) and (D), 10 μg protein was applied to each lane. Skp2, actin, Rab3, and PSD-95 are loading controls.
(E) Cartoon of GFP-tagged SCRAPPER constructs. Expression was verified using anti-GFP antibody.
(F) Shown in the left column is immunofluorescence of endogenous SCRAPPER (SCR, green) and synaptophysin (red) in cultured hippocampal neurons. Shown in the right-hand side in two columns is localization of GFP-SCR shown in (E); areas white rectangular boxes are shown at higher magnification under the respective panel.

of SCRAPPER was either abolished in all tissues or enhanced within the hippocampus, respectively (Figures 3A and 3B). No overt physiological difference was observed between SCR-TG and non-TG mice (Figures 3C and 3D, right). In contrast, the genotypes of offspring from intercross of SCR-KO heterozygous parents did not conform to a Mendelian ratio (29% wild-type [WT], 52% heterozygotes, and 19% homozygotes at birth, $p < 0.01$, χ^2 goodness-of-fit t test; Figure 3C). SCR-KO progeny also died stochastically after birth and had reduced

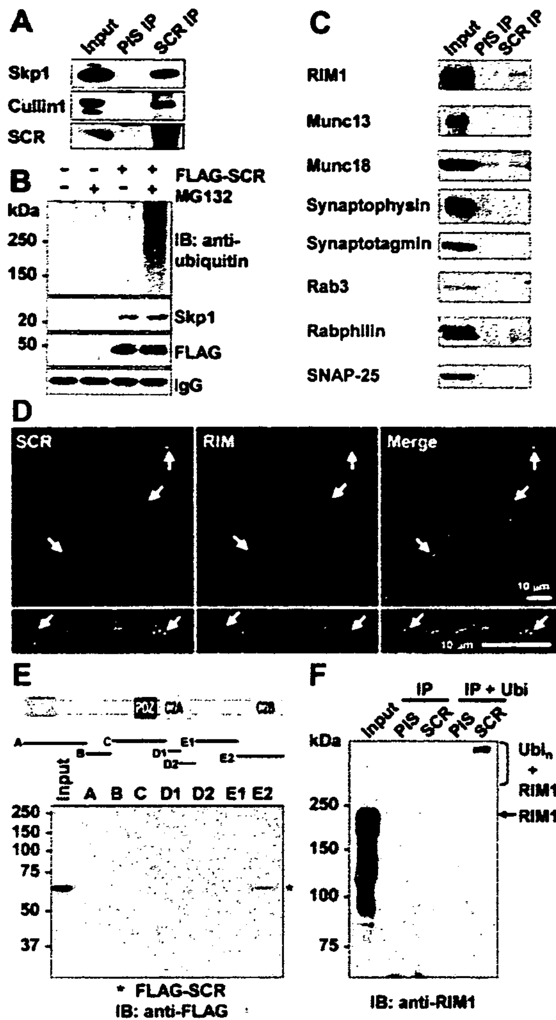

Figure 2. SCRAPPER Acts as an E3 Ligase for RIM1 In Vitro
(A) SCRAPPER forms an SCF complex in the mouse brain. Input, original tissue extract; PIS IP and SCR IP, immunoprecipitates generated using the preimmune serum (PIS IP) or with the anti-SCRAPPER antibody (SCR IP); IB, immunoblotted with indicated antibody.
(B) Extract of HEK293T cells transfected FLAG-SCR with HA-tagged ubiquitin and treated ±MG132 was immunoprecipitated with anti-FLAG antibody, and blotted with antibodies to Ubiquitin, Skp1 or FLAG.
(C) Immunoprecipitates generated with the anti-SCRAPPER antibody from the mouse brain were blotted with the indicated antibodies. Endogenous RIM1 was coimmunoprecipitated with SCRAPPER.
(D) Immunostaining pattern of endogenous SCRAPPER (SCR; green) and RIM1 (red) in cultured hippocampal neurons. Arrows indicate examples of overlapping signals.
(E) SCRAPPER interacted with the C2B domain of RIM1.
(F) Ubiquitination of RIM1 in anti-SCRAPPER immunoprecipitates. Samples were blotted with anti-RIM1 antibody. IP + Ubi, samples to which ubiquitination-system mixture (containing ubiquitin, E1, E2, and a NEDD8 system) was added to immunoprecipitates containing SCRAPPER.

lifespan (Figure 3C) and smaller body size (Figures 3D [left], S4A, and S4B) compared to WT littermates. Necropsy of homozygous SCR-KO mice was unremarkable except for a smaller pancreas (Figure S4D).

We used SCR-KO mice to investigate SCRAPPER-dependent RIM1 ubiquitination in vivo. In hippocampal acute slices prepared from WT mice, the steady-state level of RIM1 was increased by treatment (50 μM, 1 hr) with MG132 (Figure 3E). Consistent with a role for SCRAPPER in facilitating degradation of RIM1, untreated brains of SCR-KO mice displayed increased levels of RIM1, which increased further following treatment with MG132, although the relative increase was smaller than that observed after MG132 treatment in WT mice (Figures 3E and 3F). In addition, in MG132-treated IPs from WT mice, RIM1 was shifted to a higher molecular weight, whereas this was not detected in similarly treated IPs from SCR-KO mice (see "RIM1 IP" in Figure 3E). These results indicate that SCRAPPER is the main E3 ligase for RIM1 ubiquitination in a short time window in vivo. Consistent with these findings, the half-life of RIM1 was 0.7 ± 0.1 hr in WT neurons and 5.0 ± 0.1 hr in neurons from SCR-KO mice (Figures 3G, 3H, and S5), confirming that SCRAPPER enhances the rate of turnover of RIM1. In contrast, there was no significant difference in the half-life of β-catenin, an additional synaptic protein (5.4 ± 0.3 hr, WT; 5.0 ± 0.1 hr SCR-KO; Figure S5).

SCRAPPER Regulates the Synaptic Level of RIM1 In Vivo

As the steady-state level of RIM1 was increased in SCR-KO mice, we investigated whether a supraphysiological level of SCRAPPER was sufficient to mediate a decrease in levels of RIM1 in vivo. To do so we performed western analyses of brain lysates from each SCR-TG mouse line (TG-22, TG-26, and TG-31), SCR-KO, and WT mice. Indeed, an increased steady-state level of SCRAPPER produced a reduction in the level of RIM1 as well as several presynaptic proteins, including synaptophysin and synapsin IIa in vivo (Figure 4A). The level of mRNA for presynaptic proteins such as RIM1, synaptotagmin, and SNAP-25 were unchanged in SCR-TG, SCR-KO, and WT mice (Figure S6). In conventional two-dimensional polyacrylamide gel electrophoresis (2D) analyses, almost all brain proteins in SCR-KO and in SCR-TG (data not shown) were unchanged compared with those of WT animals. Thus, the changes of RIM1 protein level in the SCR-KO brain were specific.

Immunofluorescence analyses of SCR-KO hippocampi revealed that the increased level of RIM1 occurred in the synaptic region, not in the cell body (Figures 4B, 4C, and S7). Conversely, the intensity of RIM-specific fluorescence in the synaptic region was reduced in SCR-TG hippocampi relative to that of WT (Figures 4B, 4C, and S7). In parallel, we assessed the distribution and number of synapses of the SCR-KO mice. No significant difference was observed in the number of synapses per neurite length (Figure 4G) between WT and SCR-KO neurons.

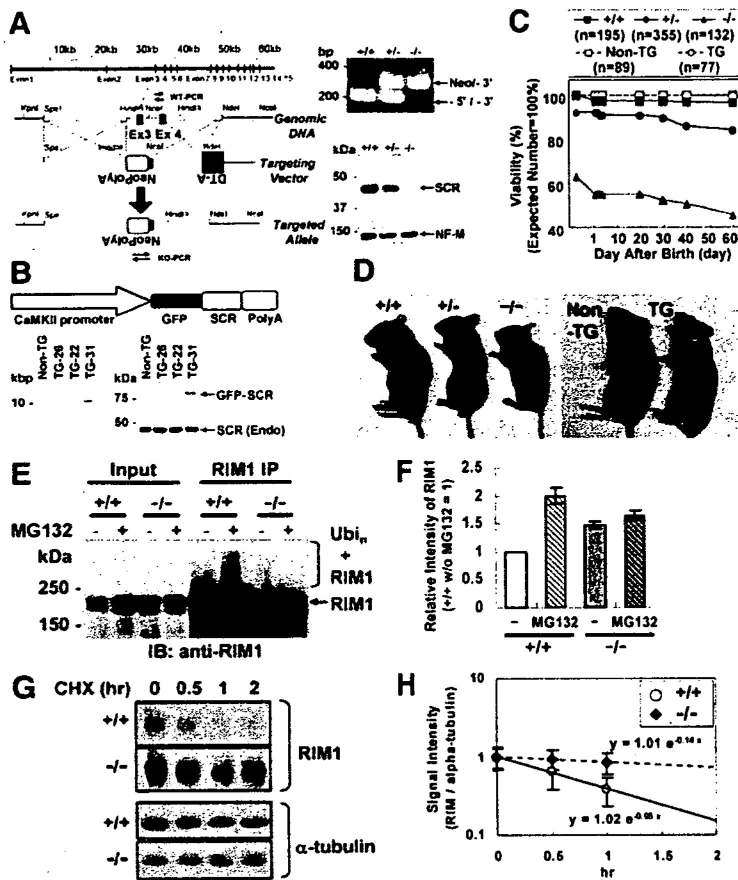

Figure 3. SCRAPPER-Dependent UPS Ubiquitinates RIM1 In Vivo

(A) Targeted disruption of the *Scrapper* gene. Right panels show PCR genotyping and western analysis using anti-SCRAPPER antibody. Neurofilament-M (NF-M) is a loading control.

(B) Upper, cartoon of the transgene; lower panels, Southern blot analysis of genomic DNA from hemizygous mice of indicated TG lines and detection of transgene products using anti-SCRAPPER antibody.

(C) Longevity of SCR-KO mice. Expected ratio of genotypes was based on simple Mendelian rules of inheritance.

(D) Appearance of SCR-KO (left panel) and SCR-TG-31 (right panel) mice.

(E) Ubiquitinated RIM1 was detected in anti-RIM1 immunoprecipitates prepares from acute slices of the WT mice brain treated ±MG132 (50 μM, 1 hr) but not in samples from SCR-KO. Input, original extract; RIM1 IP, immunoprecipitates generated with anti-RIM1 antibody.

(F) Quantification of the relative intensity of RIM1 signal in panel (E), input. Values are means ± SEM (standard error of the mean), n = 3.

(G and H) Increased half-life of RIM1 in SCR-KO neurons. Cultured neurons of cerebral cortex at 7 days in vitro were treated with 20 μg/ml cycloheximide (CHX, a translational inhibitor) for the indicated time period. Values are average signal intensity (means ± SEM, n = 4) of RIM1 compared to signal intensity of α-tubulin and normalized to 1 at time "0." +/+, WT; +/−, heterozygote; −/−, homozygote SCR mutant mice.

Analysis of the hippocampal CA1 region by transmission electron microscopy (TEM) revealed an increased local density and fewer docked synaptic vesicles in SCR-KO neurons (Figures 4D–4F), although the total number of synaptic vesicles was unchanged (Figure 4F). The number of synapses and the sizes of the active zones were also similar in WT and SCR-KO mice (Figure 4F).

SCRAPPER Is a Regulator of Presynaptic Vesicle Release

As RIM1 is known to regulate synaptic transmission (Wang et al., 1997), we investigated whether altered levels of RIM1 and morphological changes of synaptic vesicles in SCR-KO mice was associated with altered neural transmission. We analyzed AMPA-receptor-mediated miniature excitatory postsynaptic currents (mEPSC) from SCR-KO hippocampal primary culture (Inoue et al., 2006). The mEPSC frequency was increased in neurons from SCR-KO mice compared to WT littermates, and the increment was corrected by exogenous re-expression of SCRAPPER (WT; 0.91 ± 0.23 Hz, n = 15, SCR-KO; 3.05 ± 1.12 Hz, n = 14, SCR-KO-rescue; 0.98 ± 0.27 Hz, n = 10) (Figures 5A and 5B). Thus, SCRAPPER plays a significant role in regulation of neurotransmitter release.

To further investigate the functions of SCRAPPER in synaptic transmission via RIM1 ubiquitination, we expressed various forms of GFP-SCRAPPER (Figure 1E) or nontagged red fluorescent protein (RFP) in primary hippocampal neurons (Figure 5C). To determine if SCRAPPER was acting at the pre- or postsynaptic site, we cocultured neurons expressing the various GFP-SCR constructs with neurons expressing only nontagged RFP and recorded mEPSCs. Neurons transfected with GFP-SCR exhibited significant decrease in frequency but not amplitude of mEPSC, whereas the expression of either GFP-SCR-C435A (CAAX mutation) or GFP-SCR-CAAX, which lacks the RIM1 binding domain, had no significant effect on the frequency and amplitude of mEPSC (Figures 5D and 5E). In contrast, neurons transfected with GFP-SCR-LRR, in which we expected a dominant-negative effect caused by binding of the LRR to RIM1, exhibited increased mEPSC frequency but not amplitude (Figures 5D and 5E). Recording of mEPSC from RFP (i.e., non-SCR)-transfected cells in the mixed culture showed the same significant change in mEPSC, demonstrating that the SCRAPPER-dependent effect on neurotransmitter release was generated at the presynaptic site.

Because RIM1 is a known component of a Ca^{2+} sensor (Sudhof, 2004), we tested the Ca^{2+} sensitivity of neurons

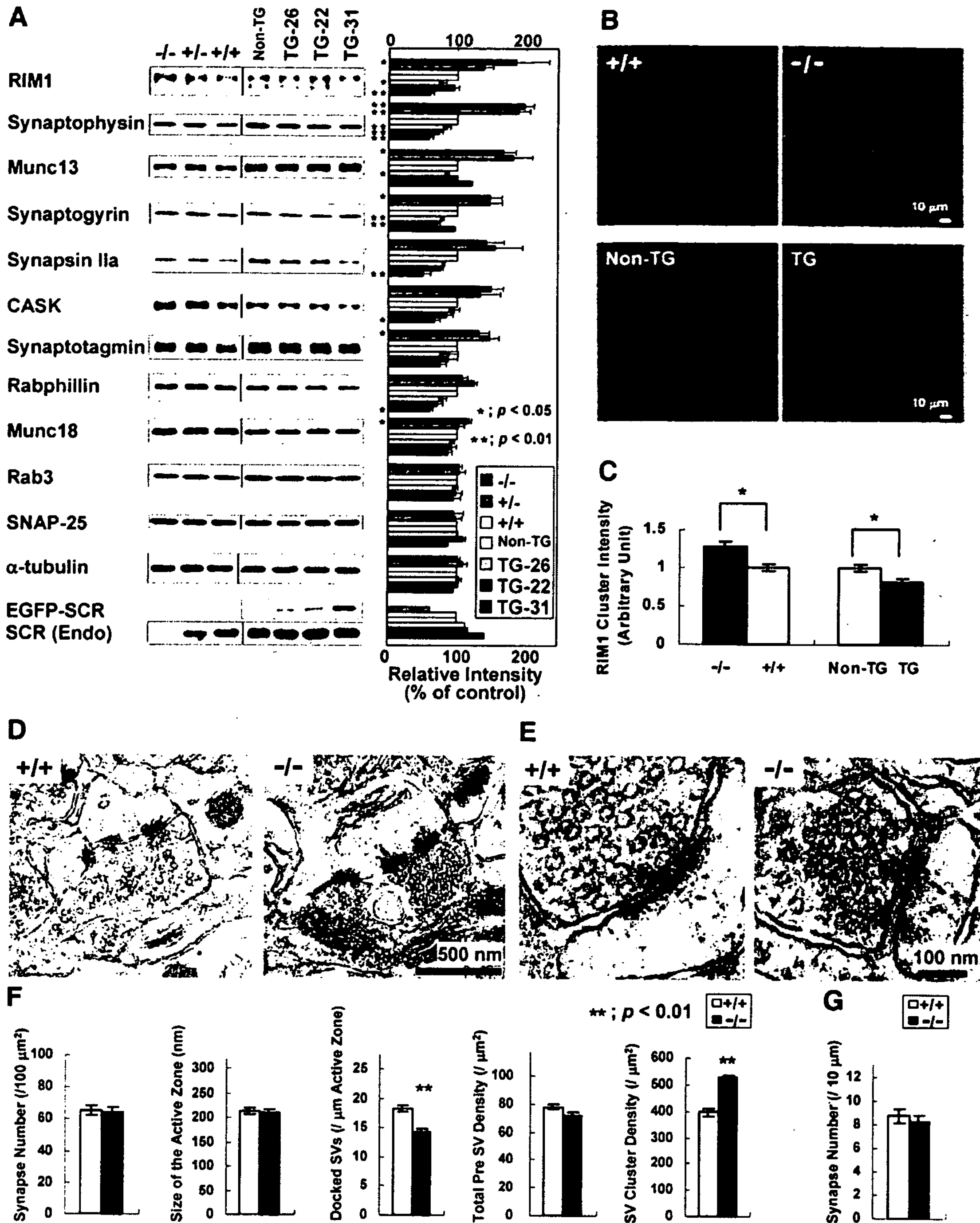

Figure 4. Inverse Relationship between Steady-State Levels of SCRAPPER and a Subset of Presynaptic Proteins In Vivo
(A) Western analysis of SCRAPPER mutant mice. Five μg or 0.5 μg protein of whole brain homogenate was applied to each lane. Values for WT are set at 100%. Three independent animals were analyzed.
(B) Immunofluorescence analyses of hippocampal neurons from WT (+/+), SCR-KO (−/−), non-TG, and SCR-TG-31 (TG) animals labeled with mAb to RIM1 (green) and TOTO-3 (nuclei, blue).
(C) Quantitative analysis of the RIM1 clusters intensity on the panel (B).
(D and E) Representative TEM images of hippocampal CA1 region of WT (+/+) and SCR-KO (−/−) mice.
(F) Quantification of synapses to apical dendrites in the distal stratum radiatum of the hippocampal CA1 region in WT and SCR-KO mice using TEM,

expressing altered forms of SCRAPPER. The effect of expression of SCR forms on modulating mEPSC frequency was observed in the presence of 5 mM but not 10 mM or 20 mM extracellular Ca^{2+} (Figure 5F). Similar results were also observed in the case of evoked-field EPSP (fEPSP) at the hippocampal acute slice preparations (Figures S8A–S8C). We verified that the intracellular Ca^{2+} level of SCR-KO neurons was within the normal range in assays by using Fura2 or a FRET-based Ca^{2+} indicator (Miyawaki et al., 1999) (Figures S8D and S8E). These results indicate that SCRAPPER can regulate the Ca^{2+} sensitivity in presynaptic machinery.

SCRAPPER Regulates Synaptic Vesicle Release via RIM1 and Proteasome Activity

To determine if the altered mEPSC frequency in SCR-KO neurons is mediated specifically via RIM1, we knocked down expression of RIM1 in SCR-KO neurons and analyzed if this was sufficient to rescue the SCR-KO phenotype. Indeed, reduction of RIM1 in SCR-KO neurons was sufficient to rescue the increased frequency of mEPSC (Figures 6A–6C). These results demonstrate that mEPSC frequency can be regulated via SCRAPPER-mediated RIM1 degradation. Overexpression of RIM1 promoted neurotransmitter release (Figures 6D and 6E), which mimicked the SCR-KO phenotype, indicating that the increased RIM1 in SCR-KO mice is sufficient to account for the mEPSC phenotype.

To evaluate the relative contribution of SCRAPPER to UPS-mediated degradation of proteins in neurons, we recorded mEPSC from SCR-KO in the hippocampal CA1 pyramidal neurons in acute slices and analyzed the effect of treatment with MG132 or epoxomicin, another proteasome inhibitor. Significantly, the effect of proteasome inhibitors on mEPSC frequency in acute slices prepared from WT mice was mostly abolished in samples from SCR-KO mice (2.1-fold in WT to 1.2-fold in SCR-KO [MG132 treatment]; 1.9-fold in WT to 1.2-fold in SCR-KO [epoxomicin treatment]; Figure 6H). In contrast, MG132 had no effect on amplitude of mEPSC between SCR-KO and WT mice (Figures 6F–6H).

We investigated the SCRAPPER-proteasome effect on mEPSC not only in acute slices but also in primary cultures of dissociated neurons. When we applied MG132 (50 μM) to primary cultured hippocampal neurons, the frequency and amplitude of mEPSC was increased within 60 min (Figure S9). In contrast, neither amplitude nor frequency of mEPSC was altered following treatment of neurons with the calpain inhibitor ALLM (Figure S9). The mEPSC upregulated by MG132 was completely suppressed under extracellular Ca^{2+}-free conditions and was diminished at higher Ca^{2+} conditions (Figures 6I and 6J). The increase in mEPSC frequency by proteasome inhibitor and the poor response to MG132 in SCR-KO neurons were also demonstrated in the dissociation cultures (7.2-fold in WT to 2.1-fold in SCR-KO, Figure S10).

Altered Short-Term Synaptic Plasticity in SCR-KO Mice

RIM1 mutant mice have increased paired-pulse facilitation (PPF) (Schoch et al., 2002), which is a form of short-term synaptic plasticity (STP) (Katz and Miledi, 1968). Thus, we predicted the PPF in SCR-KO would be affected. We analyzed PPF from the CA3-CA1 synapse of the hippocampal acute slice preparation (Figure 7). The PPF ratio was significantly reduced in SCR-KO mice at every stimulation interval (50, 100, 200, 300, 400, and 500 ms) tested (Figures 7A and 7B). Furthermore, a gradual increase in fEPSP slope and decrease in PPF ratio was observed during treatment of neurons with 50 μM of MG132 for 20 min, and this effect became saturated after 1 hr in both WT and SCR-KO mice (Figures 7C–7E). The effect of exposure to MG132 on fEPSP slope was significantly smaller in SCR-KO mice than in WT mice (normalized fEPSP slope after 1 hr MG132 treatment; 1.31 ± 0.05 in WT, n = 7, versus 1.14 ± 0.04 in KO, n = 7). As with alteration of the mEPSC frequency by MG132 in SCR-KO neurons, the effect of MG132 on the PPF ratio was significantly smaller in SCR-KO mice (i.e., a change from 1.61 ± 0.06 at −10 to 0 min before the application of MG132 to 1.36 ± 0.08 after 1 hr of MG132 treatment, n = 7) compared to WT mice (1.94 ± 0.05 at −10 to 0 min before the application of MG132 to 1.41 ± 0.10 after 1 hr of MG132 treatment, n = 7) (Figures 7D and 7E). These results demonstrate that SCRAPPER can regulate presynaptic STP.

DISCUSSION

SCRAPPER Is an E3 Ligase on Synaptic Membranes

We used bioinformatics to identify SCRAPPER, a neuronal and membranous ubiquitin ligase. SCRAPPER was the only protein identified by our strategy to screen for F box containing proteins that could be membrane localized and whose expression is predicted in neurons. Among the 68 F box protein-coding genes in the human genome (Jin et al., 2004; Winston et al., 1999), *SCRAPPER* is one of six independent genes that have orthologs in *C. elegans*, *D. melanogaster*, and mammals (data not shown), which suggests that it might function as an important membrane-localized E3 ligase in various species. SCRAPPER is broadly expressed within the mouse CNS and is abundant at the presynaptic membrane. Many E3s have been identified whose activities are localized to specific

determined from a total of 230 asymmetrical synapses containing small spherical vesicles and with dense postsynaptic zone from three animals of each genotype.
(G) Quantification of the synapse number per 10 μm neurites of hippocampal neurons. SV, synaptic vesicle. In (A)–(G), data are expressed as means ± SEM. TG, transgenic; +/+, wild-type; −/−, homozygote. *p < 0.05; **p < 0.01 (t test).

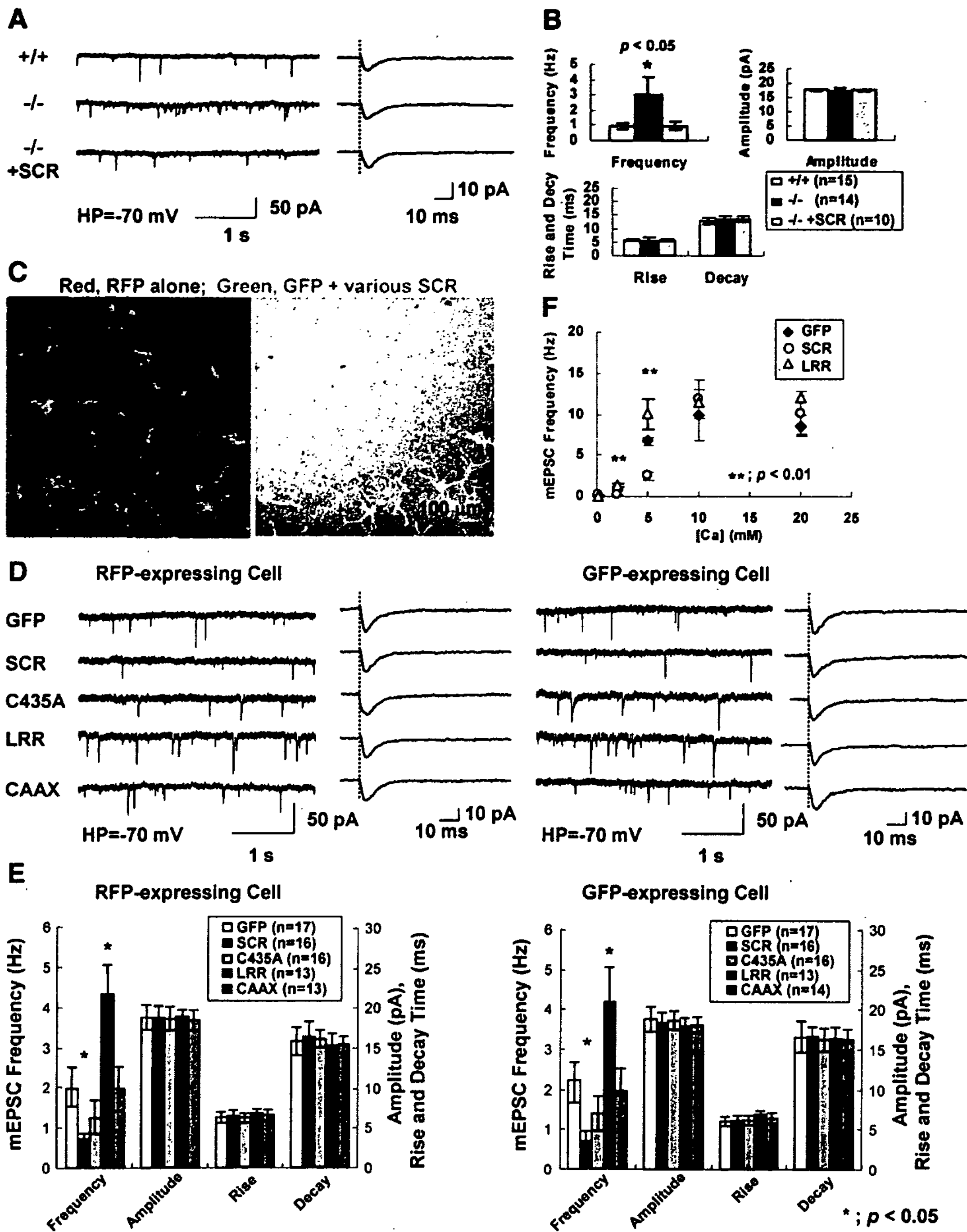

Figure 5. SCRAPPER-Mediated UPS Functions in Presynaptic Transmission

(A) Analysis of mEPSC from hippocampal cultures of SCR-KO (−/−) mice. Representative mEPSC traces for 4 s are in the left column and averaged mEPSC traces are in the right column.

(B) The frequency of mEPSC was significantly increased in the SCR-KO neuron, and the effect was suppressed by re-expression of SCRAPPER.

(C) Representative picture of mixed culture. Rat hippocampal neurons expressing GFP-SCR shown in Figure 1E were cocultured with (control) neurons expressing only nontagged RFP. Right panel is the merge of FL and DIC.

(D) mEPSC was recorded from the nontagged RFP- or GFP-expressing neurons in each group of cocultured neurons. Representative mEPSC trace is in the left column and averaged mEPSC trace is in the right column.

subcellular compartments such as nuclei or cytoplasm, for the regulation of transcription or cell cycles (Coux et al., 1996; Hershko and Ciechanover, 1998).

RIM1 Is a Target of SCRAPPER

Experimentally, SCRAPPER behaves as an F box type E3 ligase and RIM1 is a target of SCRAPPER in the mouse brain. Under normal circumstances, UPS-targeted multiubiquitinated RIM1 are rarely detected due to their rapid turnover. This may account for the relatively weak signal observed of coIPed RIM1. Consistent with this prediction, the RIM1-specific signal was shifted upward after in vitro ubiquitination. At present, we cannot exclude the existence of additional SCRAPPER targets in the synapses. Indeed, many E3 enzymes recognize several substrates as a target (Hatanaka et al., 2006b; Ingham et al., 2004).

RIM1 plays an important role in the vesicle priming step in the active zone of the presynapse (Betz et al., 2001; Kaeser and Sudhof, 2005). Recently, we reported that SAD kinase, which can phosphorylate RIM1, is expressed at presynapses and can regulate synaptic transmission (Inoue et al., 2006). Among the F box protein family, the binding of some LRR-type F box proteins to substrates can be influenced by phosphorylation (Hsiung et al., 2001). Because SCRAPPER may recognize the phosphorylation of the substrate as predicted from the leucine-rich sequence, it is possible that SCRAPPER and SAD cooperatively regulate synaptic transmission and plasticity via modulation of RIM1.

Reduction of RIM1 Ubiquitination and Increased Levels of RIM1 in Presynapses in SCR-KO Mice

Analysis of SCR-KO mice revealed that SCRAPPER regulates steady-state level of RIM1. RIM1 degradation can also be controlled via SCRAPPER-independent mechanisms as treatment with MG132, a proteasome inhibitor, produced a further increase in levels of RIM1 in SCR-KO mice. However, the majority of RIM1 degradation appears to be SCRAPPER dependent. This conclusion is supported by the fact that the lifetime of RIM1 was seven times greater in neurons from SCR-KO compared to WT mice. Interestingly, the levels of several presynaptic-localized proteins such as synaptotagmin were also inversely proportional to steady-state level of SCRAPPER in vivo, although the mRNA levels of these presynaptic proteins were unchanged. A 2D analysis indicated that relatively few proteins were affected by the absence of SCRAPPER. This suggests that stabilization of RIM complex proteins in SCR-KO mice impacts relatively few proteins.

Although the sizes of the active zones were unchanged in SCR-KO mice, we found several presynaptic morphological phenotypes such as an increased density of synaptic vesicles and reduced number of docked vesicles. How increased RIM1 generates these morphological phenotypes is not immediately apparent as the synaptic morphology in RIM1-mutant mice does not involve alteration in localization or density of synaptic vesicles (Schoch et al., 2002). The multidomain structure of RIM1 complicates reconciliation of phenotypes in gain- and loss-of-function mice. It is possible that altered expression of presynaptic proteins other than RIM1 contribute to the altered synaptic morphology in SCR KO.

We found no difference in the number and basic structure of synapses in either cultured neurons or hippocampal CA1 region in SCR-KO and WT mice, suggesting that SCRAPPER had no overt effect on synapse development. In contrast, other neural E3 ligase such as *Drosophila* Highwire, the *C. elegans* homolog RPM-1, and the mammalian proteins Phr1 and Pam, constitute a conserved family of proteins, all of which influence synapse development (DiAntonio et al., 2001; McCabe et al., 2004). Additional, as yet unknown E3 ligases may exist that can regulate synaptic development in mammals.

SCRAPPER Is an Important Regulator of Synaptic Transmission

Electrophysiological analyses verified that SCRAPPER can regulate synaptic transmission, especially neurotransmitter release. Recording of mEPSC frequency in mixtures of neurons expressing either nontagged RFP or GFP displayed no significant difference between cells. In contrast, changes observed when recording from nontagged RFP-positive cells in the presence of GFP-positive neurons transfected with different GFP-SCR constructs were interpreted as an effect generated in the presynaptic (green) cell. Use of this strategy (suggested by a reviewer) enabled us to clarify the importance of SCRAPPER function at the presynaptic site. The synapses of neurons expressing elevated levels of SCRAPPER displayed a lower mEPSC frequency via lower Ca^{2+} sensitivity. In contrast, neurons expressing SCR-LRR (RIM1-binding domain) showed a higher Ca^{2+} sensitivity, most likely as a consequence of the dominant-negative effect of this protein. This indicates that SCRAPPER can regulate neurotransmitter release in a LRR domain-dependent manner. This effect was not significantly observed in cells overexpressing SCR-CAAX. Cells expressing SCR-C435A, where the cysteine in the canonical CAAX prenylation motif is replaced by alanine, displayed an intermediate reduction in the frequency of mEPSC, though this was a trend and not statistically significant. One possible explanation why mutation of the cysteine residue diminished SCR activity only moderately is this sequence was able to target SCR to membranes with reduced efficiency.

(E) The frequency of mEPSC recorded from either the nontagged RFP- or GFP-expressing neurons both significantly decreased in GFP-SCR group and increased in GFP-LRR group.
(F) Dependence of extracellular Ca^{2+} concentration on the frequency of the mEPSC. In (B), (E), and (F), data are expressed as means ± SEM. *$p < 0.05$; **$p < 0.01$ (t test).

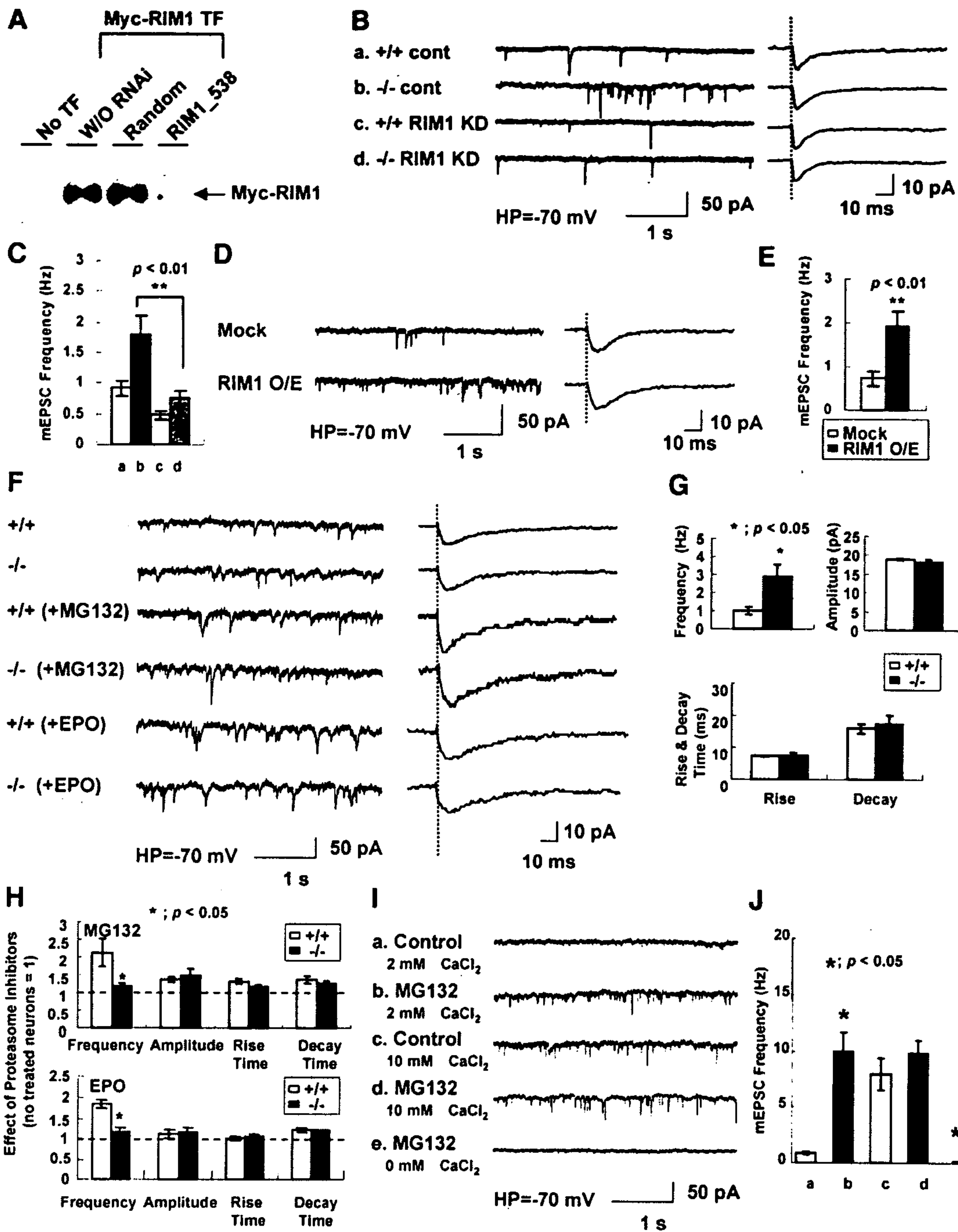

Figure 6. SCRAPPER Tunes Synaptic Transmission via Regulation of RIM1
(A) Western blot analysis of the high efficiency of the knockdown of RIM1with 293T cells ± a vector expressing RNAi against RIM1 (RIM1_538). TF; transfected.
(B) Representative traces of mEPSC from SCR-KO cultured neurons treated ± RIM1-RNAi.
(C) Quantification of mEPSC frequency in (B). Horizontal axis labels correspond to notations in (B).
(D) Representative traces of mEPSC from rat hippocampal cultured neurons transfected with RIM1. O/E, overexpressed.
(E) Comparison of mEPSC frequency in (D).
(F) mEPSC was recorded from CA1 hippocampal neurons of SCR-KO slices (±MG132 [50 μM, 1 hr] or Epoxomicin [10 μM, 1 hr] treatment) under voltage clamp conditions. Representative mEPSC trace (left column); averaged mEPSC trace (right column).
(G) The frequency of mEPSC was significantly increased in the SCR-KO slices compared to the WT.

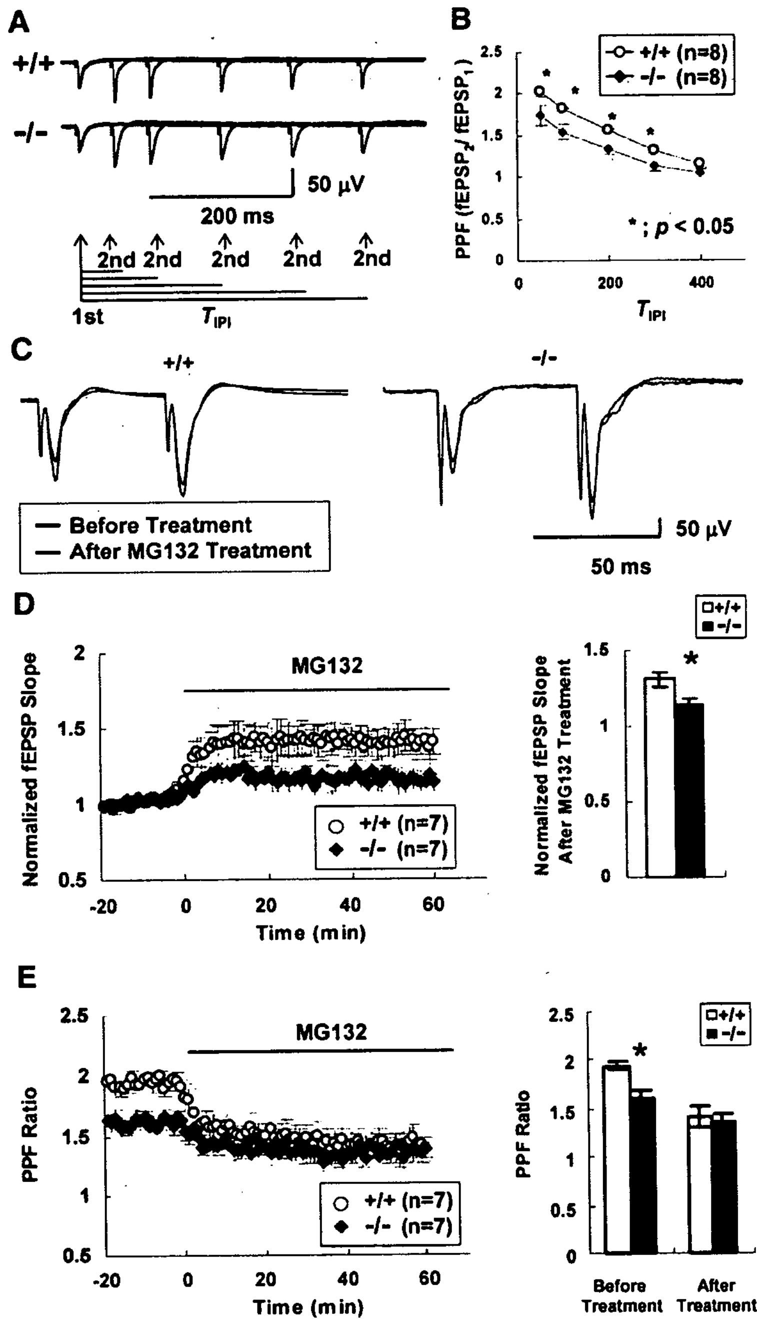

Figure 7. SCRAPPER Functions in Short-Term Synaptic Plasticity

(A and B) PPF ratios of the subsequent and initial fEPSP slopes (interpulse interval: 50, 100, 200, 300, and 400 ms). Data are expressed as means ± SEM.

(C)–(E) Alternation of PPF ratios of the subsequent and initial fEPSP slopes (interpulse interval: 50 ms) recorded from hippocampal slices of WT or SCR-KO mice after treatment with MG132. In (D) and (E), data. recorded at 1 min stimulation intervals are expressed as mean ± SEM. $^*p < 0.05$ (t test).

Further experiments are required to discriminate between this and other possibilities. It is possible that the increased mEPSC frequency reduced the number of docked vesicles observed by electron microscopy, and the rate of supply of newly synthesized synaptic vesicles to active zones is unable to support the consumption of synaptic vesicles at the increased mEPSC frequency, although other explanations are possible.

(H) Effect of MG132 (50 μM, 1 hr) or Epoxomicin (10 μM, 1 hr) on mEPSC parameters from the hippocampal slices of WT or SCR-KO mice (n = 3).
(I and J) Representative traces of mEPSC from cultured neurons ± MG132 treatment (50 μM, 1 hr) at 0, 2, or 10 mM Ca^{2+} concentration (I) and comparison of mEPSC frequency (J). Horizontal axis labels in panel (I) correspond to the notations in panel (J). Data are expressed as means ± SEM in (C), (E), (G), (H), and (J). $^*p < 0.05$; $^{**}p < 0.01$ (t test).